

Technical Paper

Evaluation of critical crack width for reinforcement corrosion in RC member based on numerical simulation of transport of chloride ions in concrete

Nguyen Thi Hien* and Takumi Shimomura

(Received: July 15, 2017; Accepted: November 13, 2017; Published online: January 5, 2018)

Abstract: Chloride-induced reinforcement corrosion in reinforced concrete structures exposed to marine environment is one of the most important factors affecting the durability of structures. To minimize the effect of cracks on the deterioration of RC structures, current design codes often limit the crack width. However, recent investigations indicated that condition of steel-concrete interface is a more essential criterion related to reinforcement corrosion. The purpose of this study is to clarify the effect of various conditions including cover thickness, water-cement ratio, environment action and interfacial void on limitation of crack width. The validity of crack width limitation in design codes is discussed based on analytical results.

Keywords: crack width limitation, chloride ingress, bleeding, interfacial void, flexural crack.

1. Introduction

Corrosion of reinforcing bars in concrete due to chloride penetration is one of the main causes of deterioration of reinforced concrete structures under marine environment. Reduction of chloride penetration is, therefore, crucial to the design and construction of concrete structures under load and environmental action. RC structures are in general allowed to have flexural cracks under the service load. The effect of flexural crack on chloride penetration into concrete has been studied by many researchers [1-5]. It has been confirmed that chloride ingress into concrete increases with increasing surface crack width.

The influence of crack width on corrosion initiation has been investigated by many researchers [6-9]. It has been clarified that the risk of corrosion initiation increases with increasing crack width. Therefore, to ensure design service life of RC structure, crack width should not exceed the threshold value to avoid corrosion risk of embedded steel due to chloride. In several studies [10-18], efforts were made to determine the threshold value of crack width. Table 1 summarizes literatures which proposed the critical crack width for reinforcement cor-

rosion. It was found that critical crack width is not a unique value depending on the definition of initiation of corrosion. While a value of 0.1 mm was reported by Schiessl [11], O'neil [14] found a value of 0.4 mm and it was expressed as a function of cover thickness by Yachida [17].

Table 1 – Limitation of crack width for reinforcement corrosion

Researcher	Limitation of crack width (mm)
Shiessl.,P.,Rehm, G [10,11]	0.1
Shalon, R [12]	0.15
Okada.K and Miyagawa .T. [13]	0.1-0.2
O'neil.E.F [14]	0.4
Kamiyama [15]	0.01
Maruyama and Seki [16]	0.2
Yachida [17]	0.0065c-0.14c
Kamiyama [15]	0.1

NOTE: c – cover thickness (mm)

Steel-concrete interface in RC member such as girder bridge, slab bridge, and highway pavements, is generally damaged due to increased tensile stress or cyclic load. The defect of steel-concrete interface is also caused by concrete bleeding resulting in the formation of interfacial void around reinforcing bar. The influence of defect of steel-concrete interface on corrosion initiation has been confirmed in a few studies [19-26]. Mohammed [19] found that the presence of gaps/voids at the steel-concrete interface causes the complete loss of passivity with the

Corresponding author Nguyen Thi Hien is a Ph.D. Student, Graduate School of Engineering, Nagaoka University of Technology, Niigata, Japan.

Takumi Shimomura is a Professor, Department of Civil and Environmental Engineering, Nagaoka University of Technology, Niigata, Japan.

presence of chloride and, therefore, it is necessary to make concrete without interfacial void at steel-concrete interface to ensure long-term durability of RC structures. Savija [20] found that the defect of steel-concrete interface was an important factor in chloride ingress and subsequent reinforcement corrosion. A. Castel [21] showed that the quality of steel-concrete interface is greatly dominant in prediction of the initiation of corrosion in reinforced concrete members. T.A Soylev [22] concluded that damage of steel-concrete interface affected directly to the corrosion rate. Interaction between flexural crack and interfacial void has been investigated in the author's previous studies [27, 28]. The authors found that chloride ingress into concrete with flexural crack was promoted with presence of interfacial void, therefore, defect around reinforcement due to bleeding should be avoided to make crack width control in RC member effective.

Several current structural codes [29-34] specify the allowable crack width with respect to environmental conditions and cover thickness. Threshold value of crack width varies among the codes due to different criteria. For example, in the standard specification (2002) for concrete structures by Japan Society of Civil Engineering (JSCE) [29], limitation of crack width is experimentally determined considering various influencing factors on corrosion as concrete cover, environmental condition, design life, type of reinforcement, in addition to chloride concentration. In CEB-FIP Model Code 1990 [30], crack width limitation is determined to ensure that steel bar will not be depassivated during anticipated service life. In the ACI 318 [32], maximum crack widths result from expected loads on the structure. Though this limitation of crack width has been proved adequate practically, its reasonableness has not been theoretically confirmed.

Based on aforementioned reasons above, the purpose of this study is to clarify the effect of

various conditions including cover thickness, water-cement ratio, environment action and interfacial void on limitation of crack width. The validity of crack width limitation in various standards will be discussed based on analytical results.

2. Method of numerical simulation

2.1 Modeling of concrete cover with flexural crack

Numerical simulation of transport of water and chloride in concrete cover was carried out to investigate the influence of flexural crack on chloride ingress into RC members and its interaction between the interfacial void around reinforcement. The layout of a part of RC member with flexural crack and the interfacial void is shown in Fig. 1, in which L is crack interval, w is crack width, v_w is width of interfacial void, c is thickness of concrete cover. Variation of crack width along the crack depth, which may exist in actual flexural crack in reinforced concrete members, was not considered in the calculation in this study. In addition, though actual crack surface is rough and crack path is tortuous, crack is assumed straight in the calculation in this study. Water and chloride ions are assumed to penetrate into concrete from the exposed surface, the crack surface and the surface of the interfacial void around reinforcement.

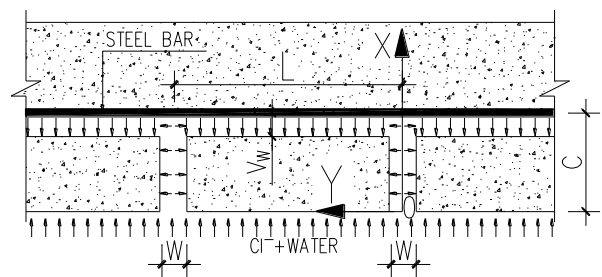


Fig. 1 - Layout of RC member with flexural crack and interfacial void

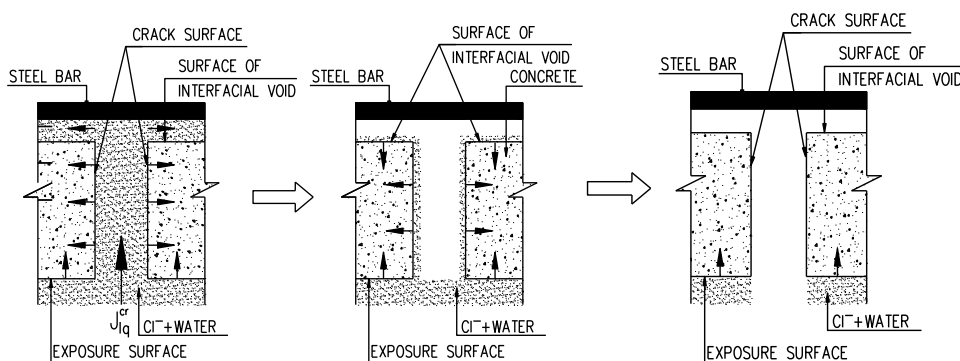


Fig. 2 - Penetration of liquid water into crack and interfacial void around reinforcement

When concrete surface directly contacts with liquid water, liquid water penetrates into crack and interfacial void around reinforcement by capillary suction. Liquid water penetrates into concrete from three surfaces: the exposed surface, the crack surface and the surface of interfacial void around reinforcement. The amount of penetrated water into concrete from the crack surface and the surface of interfacial void around reinforcement does not exceed the amount of water in the crack and the void respectively. After the crack and the interfacial void have become empty, liquid water penetrates into concrete only from the exposed surface as shown in Fig. 2.

To solve governing equations numerically, a computer program developed by the authors was used [38]. Drying process was calculated by implicit FDM (Finite Difference Method). Wetting process was calculated using an integral solution of capillary suction model. Transport of chloride ions was calculated by explicit FDM.

2.2 Transport of water in concrete

Transport of water in nonsaturated concrete is calculated by the computational model based on pore size distribution function and microscopic thermodynamic behavior of water in pore structure [35].

Pore size distribution of concrete is modeled by following function:

$$V(r) = V_0 [1 - \exp(-Br^C)] \quad (1)$$

where $V(r)$ is accumulated pore volume whose radius is not greater than r in unit concrete volume (m^3/m^3), V_0 is the total volume of pores per unit concrete volume (m^3/m^3), r is pore radius (m), B is parameter for pore size distribution, C is parameter for pore size distribution.

The mass conservation equation of water in nonsaturated concrete is expressed as:

$$\frac{\partial w}{\partial t} = -\text{div}(J_v + J_l) \quad (2)$$

where w is mass concentration of water per unit concrete volume (kg/m^3), t is time (s). The mass flux of vapour J_v and the mass flux of liquid water J_l in nonsaturated concrete are respectively calculated by the following equations.

$$J_v = -K_v V_g D_{vo} \text{grad} \rho_v \quad (3)$$

$$J_l = \int_0^{r_s} \rho_l \frac{dV(r)}{dr} \left\{ -K_l \frac{r^2}{8\mu} \text{grad} \left(-\frac{2\gamma}{r_s} \right) \right\} dr \quad (4)$$

where K_v and K_l is non-dimensional material factor for transport of vapour and liquid water respectively, V_g is volume fraction of gas phase per unit concrete volume (m^3/m^3), D_{vo} is diffusivity of vapour in free space (m^2/s), ρ_v and ρ_l are density of vapour and liquid water respectively, r_s is pore radius where the liquid-gas interface is developed (m), μ is viscosity of liquid water ($\text{Pa}\cdot\text{s}$), γ is surface tension of liquid water (N/m).

2.3 Penetration of liquid water into concrete within crack and interfacial void

The mass flux of liquid water into concrete from the concrete surface (J_{lp}) by capillary suction is evaluated by following model [36]:

$$J_{lp} = \int_{r_a}^{\infty} \rho_l \frac{dV(r)}{dr} \left\{ K_{lp} \sqrt{\frac{r\gamma}{8\mu t_w}} \right\} dr \quad (5)$$

where K_{lp} is non-dimensional frictional coefficient depending on pore structure of concrete, r_a is minimum radius of pore where capillary suction takes place (m), t_w is time from the initiation of wetting process (s).

The mass flux of water in crack (J_{lp}^{cr}) and interfacial void (J_{lp}^{iv}) by capillary suction are evaluated respectively as:

$$J_{lp}^{cr} = \rho_l \sqrt{\frac{w\gamma}{2ft_w}} \quad (6)$$

$$J_{lp}^{iv} = \rho_l \sqrt{\frac{v_w\gamma}{2ft_w}} \quad (7)$$

where f is friction factor for transport of liquid water within crack and interfacial void ($\text{kg}/\text{m}\cdot\text{s}$), w is crack width (m), v_w is width of interfacial void (m).

2.4 Drying from the crack surface and the surface of the interfacial void

The evaporation of water from concrete surface is evaluated by the following equation [35]:

$$J_B = \frac{D(w_l)}{h} (w_l - w_{lB}) \quad (8)$$

where J_B is mass flux of water through the boundary surface ($\text{kg/m}^2/\text{s}$), w_l is water concentration of concrete at the surface (kg/m^3), w_{lB} is water concentration in equilibrium with atmosphere (kg/m^3), $D(w_l)$ is equivalent moisture diffusivity at the boundary (m^2/s), h is thickness of boundary film representing the state of humidity distribution in the atmosphere near the surface, which is 0.00075 (m) at the ordinary exposed surface.

Since humidity in crack and the interfacial void around reinforcement in concrete is considered higher than the atmosphere, the evaporation of water from the crack surface and the surface of the interfacial void should be smaller than from the ordinary exposed surface. The evaporation of water from crack surface and surface of interfacial void are assumed respectively as:

$$J_{Bcr} = \beta_{cr} J_B \quad (9)$$

$$J_{Bv} = \beta_v J_B \quad (10)$$

where J_{Bcr} is mass flux of water through the boundary surface of crack ($\text{kg/m}^2/\text{s}$), J_{Bv} is mass flux of water through the boundary surface of interfacial void ($\text{kg/m}^2/\text{s}$), β_{cr} is non-dimensional factor which represents reduction ratio of evaporation from crack surface, β_v is non-dimensional factor which represents reduction ratio of evaporation from surface of interfacial void.

The value of β_{cr} and β_v will be determined in the next chapter of this paper based on comparison of numerical analysis and experiment.

2.5 Transport of chloride ions in concrete

Transport of chloride ions in concrete is calculated with considering molecular diffusion of free chloride ions within liquid water and mass flux of free chloride ions carried by liquid water:

$$\frac{\partial C_{Clt}}{\partial t} = -\text{div} \left(J_{Cl dif} + C_{freeCl} \frac{J_l}{\rho_l} \right) \quad (11)$$

where C_{Clt} is total mass concentration of chloride per unit concrete volume, $J_{Cl dif}$ is mass flux of chloride by diffusion, J_l is mass flux of liquid water, C_{freeCl} is mass concentration of free chloride.

In this study, capillary suction from concrete surface is considered as transport mechanism of

liquid water. The max flux of chloride ions by diffusion is calculated as:

$$J_{Cl dif} = -K_{Cl} D_{Cl} \text{grad} C_{freeCl} \quad (12)$$

where K_{Cl} is non-dimensional material factor which presents the effect of narrowness and tortuosity of the pore structures of concrete, D_{Cl} is diffusivity of chloride ion in liquid water.

The transition between free and fixed chloride is calculated based on the equation proposed by Maruya et al [37]:

$$C_{Cif} = \alpha C_{Clt} \quad (13)$$

where α is fixing rate of chloride ions with cement hydrate in hardened concrete formulated as a function of C_{Clt} and the type of cement.

3 Experimental investigation and its numerical simulation

3.1 Specimen

Four reinforced concrete specimens, whose sizes are 100 mm x 200 mm x 900 mm, were prepared as shown in Fig. 3. Specimen names starting with H letter represent horizontal members and specimen names starting with V letter represent vertical member. One deformed steel bar of 13 mm in diameter was embedded in the longitudinal direction in the specimens, with 40-mm concrete cover from the top surface. Table 2 shows the mix proportion of concrete used. To emphasize the influence of bleeding, unit water of concrete was set as much as 185 kg/m^3 .

Specimens were cured being wrapped with wet mattress for 28 days in the laboratory. Thereafter, flexural cracks were induced by three-point-loading. Cracks are named C1, C2, C3, C4, and C5 as shown in Fig. 3. In specimen V1 and V2, two cracks were induced. However, since the two cracks had almost same widths with each other, only one crack in each specimen, which are named C4 and C5, were selected to measure chloride content. Crack widths measured by a crack scale are presented in Table 3. The measured crack widths are surface crack widths. In the analysis, these surface crack widths are considered as crack widths. In order to control the penetration of chloride ions into concrete, all surfaces except the exposed surface of the specimens were sealed with epoxy-type adhesive. Then, all specimens were placed in a chamber with controlled temperature and humidity and peri-

odical drying-wetting actions with mist of sodium chloride solution (5% NaCl). The length of one cycle was set one day consisting of 12 hours (1/2 day) mist containing 5% sodium chloride solution at 40°C temperature and 100% relative humidity and 12 hours (1/2 day) drying at 40°C temperature and 60% relative humidity. Though crack width may change actually by drying and wetting action in the experiment, crack width was not controlled during the exposure test.

After 65 days exposure test, specimens were taken out from the chamber and cut into 25 mm

slices. Then, samples of concrete powder were taken from around the steel bar in the slices using an electric drill. Chloride concentration in concrete was measured with a chloride ion meter. The procedure of making concrete powder sample is shown in Fig. 4.

Table 2 - Concrete mix proportion

W/C (%)	s/a (%)	kg/m ³			
		W	C	S	G
60	45	185	303	793	1,006

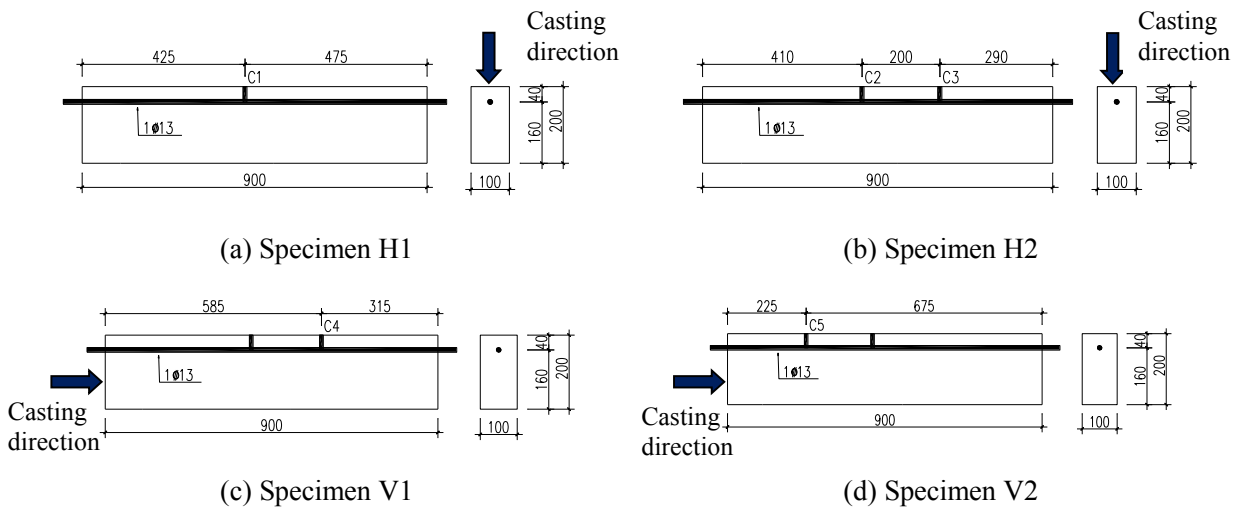


Fig. 3 – Specimen

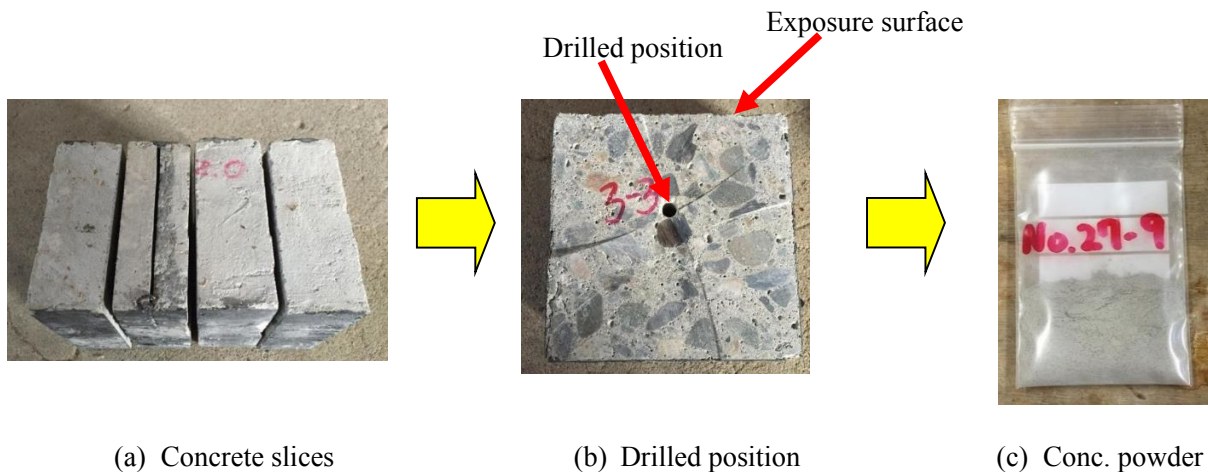


Fig. 4 – Procedure of making concrete powder samples

Table 3 - Condition of specimens

No.	Size	c (mm)	Casting direction to steel bar	Crack width, w (mm)	Drying-wetting condition (day)	Time (days)
H1	200*100*900	40	Vertical	0.75 (C1)	0.5-0.5	65
H2				0.15 (C2), 0.08 (C3)		
V1	200*100*900	40	Parallel	0.08 (C4)	0.5-0.5	65
V2				0.08 (C5)		

3.2 Test results

Figure 5 shows the experimental results of chloride concentration along reinforcing bar embedded in concrete after 65 days exposure test. It is regarded in all specimens that chloride concentration along reinforcing bar descends in accordance with the distance from crack. Chloride concentration around crack C1 whose width is 0.75 mm in specimen H1 is greater than around crack C2 whose width is 0.15 mm and around crack C3 whose width is 0.08 mm in specimen H2. This suggests that chloride ingress into concrete from crack surface is promoted by increasing of crack width. Chloride concentration around crack C1 is greater than in specimen H2. It is attributable to the existence of interfacial void around reinforcing bar due to bleeding, whose photographs are shown in Fig. 6. The influence of interfacial void on chloride ingress along reinforcing bar is greater in case of greater crack width.

Chloride concentration around crack C2 in specimen H2 in which concrete was cast in perpendicular direction to steel bar is almost same with chloride concentration around crack C4 in specimen V1 in which concrete was cast parallel to steel bar even though the crack width is same as 0.08 mm. The reason for this is that, although interfacial void due to bleeding occurred in specimen H2, liquid water did not reach reinforcing bar through crack because crack width was very small. Consequently, the influence of interfacial void is not so much when crack width is small.

Chloride concentration around crack C5 in specimen V2 is greater than around crack C4 in specimen V1 even though the crack width of both cracks are same as 0.08 mm. The reason of this is that, since concrete was cast parallel to steel bar in both specimens, concrete around crack C5 near the casting surface became more porous than around crack C4 far from casting surface due to bleeding effect.

3.3 Numerical simulation of experimental result

The values of β_{cr} and β_v are determined based on following parametric analysis. Figures 7 through 9 show distribution of calculated chloride concentration in concrete along the reinforcement near the crack, in which value of β_{cr} varied. Crack width in Figs. 7, 8, and 9 are 0.08 mm, 0.15 mm and 0.5 mm, respectively. No interfacial void is provided around reinforcement. Three values of β_{cr} shown in Figs. 7, 8, and 9 are examined for each crack width. It is clear that chloride concentration at the location of reinforcing bar increases with increasing of β_{cr} . According to the results, analytical results agree well experimental results when the value of β_{cr} is

0.04 for $w = 0.08$ mm, 0.075 for $w = 0.15$ mm and 0.25 for $w = 0.5$ mm. The relationship between crack width and obtained β_{cr} is plotted in Fig. 10. From these results, β_{cr} is modeled as a function of crack width using following formulae:

$$\begin{cases} \beta_{cr} = 0.5w \\ \beta_{cr} = 1(w \geq 2mm) \end{cases} \quad (14)$$

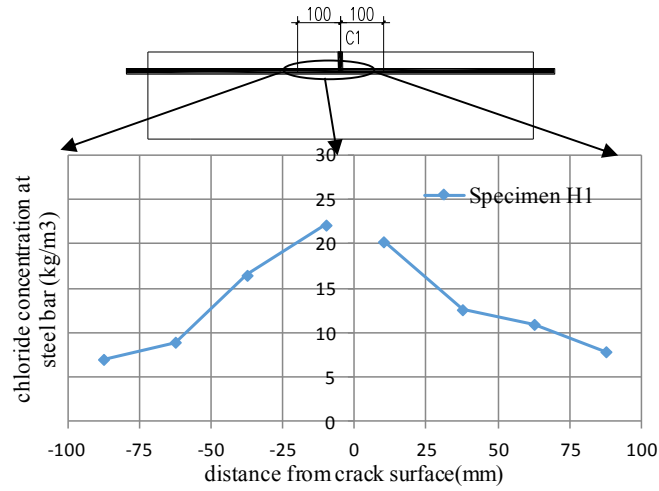
Figure 10 shows distribution of calculated chloride concentration in concrete along the reinforcement near the crack, in which value of β_v varied. Crack width is 0.75 mm and the width of interfacial void is assumed 0.02 mm. According to the results, analytical result agrees well experimental result when the value of β_v is 0.005. As there was only one experimental result with the interfacial void, the relationship between β_v and void width is assumed the same with the relationship between β_{cr} and crack width.

$$\begin{cases} \beta_v = 0.5v_w \\ \beta_v = 1(v_w \geq 2mm) \end{cases} \quad (15)$$

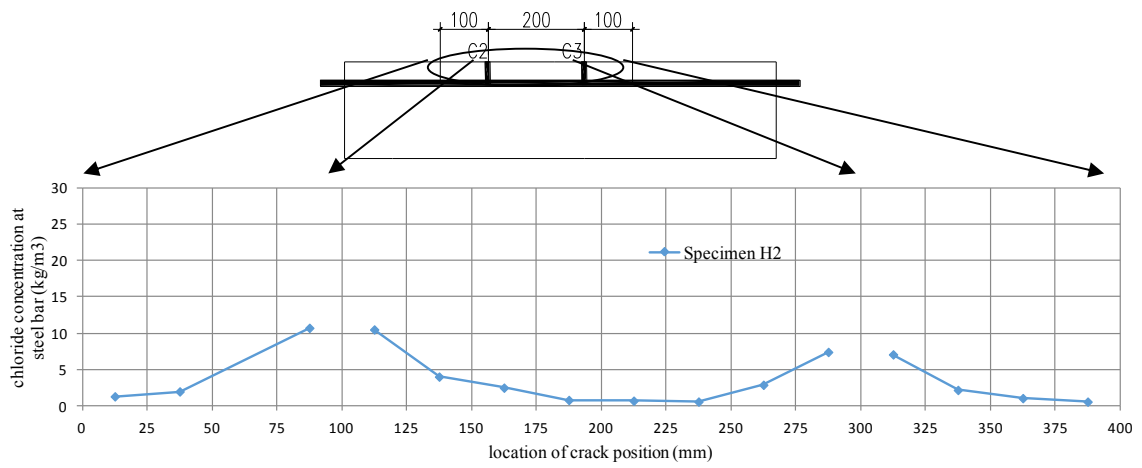
where v_w is width of interfacial void (mm).

The material parameters for transport of moisture transport and chloride ions in concrete used in the analysis are listed in Table 4. These values are determined from mix proportion of concrete based on previous studies [35, 36, and 38]. Since the portion around crack C5 in Specimen V2 may be affected by bleeding, porosity V_o in this case is assumed greater than other cases. Conditions of specimens are presented in Table 5.

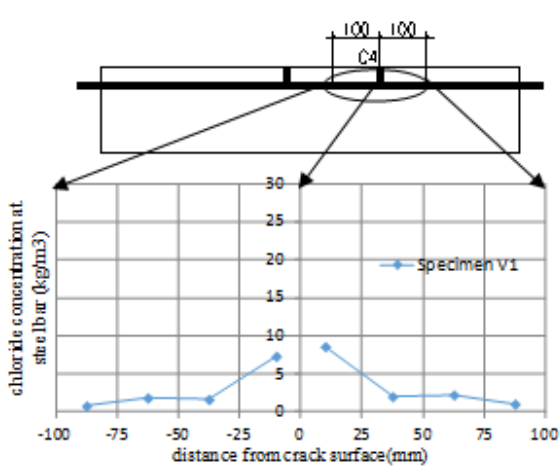
The width of the void at steel-concrete interface in specimen H1 and H2 was assumed 0.02 mm according to the measurement results by microscope, while no interfacial void was provided in specimen V1, V2. Figure 12 shows the comparison of experimental chloride distribution and analytical ones along reinforcement in concrete. The tendency of chloride distribution around cracks: C1, C2, C3, C4, and C5 are all well simulated by the analysis. The un-smoothness of chloride distribution around C1 is attributable to the effect of penetration of chloride ions from the surface of the interfacial void into concrete. The analysis can express the influence of crack and interfacial void around reinforcement observed in the experiment by determining material parameters in the model adequately.



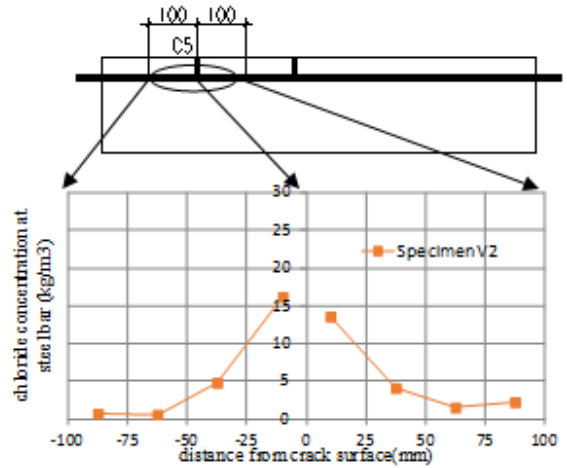
(a) C1 in Specimen H1 ($w = 0.75$ mm)



(b) C2 ($w = 0.15$ mm) and C3 ($w = 0.08$ mm) in Specimen H2



(c) C4 in Specimen V1 ($w = 0.08$ mm)



(d) C5 in Specimen V2 ($w = 0.08$ mm)

Fig. 5 - Experimental results of chloride concentration along reinforcing bar after 65 days of exposure



(a) Specimen H1,H2



(b) Specimen V1, V2

Fig. 6 - Interfacial void around reinforcement

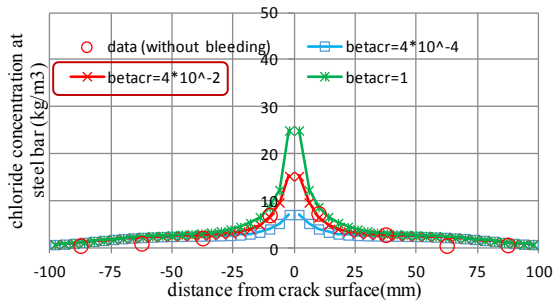


Fig. 7 - Chloride concentration along of reinforcing bar in concrete with various value of β_{cr} ($w = 0.08$ mm)

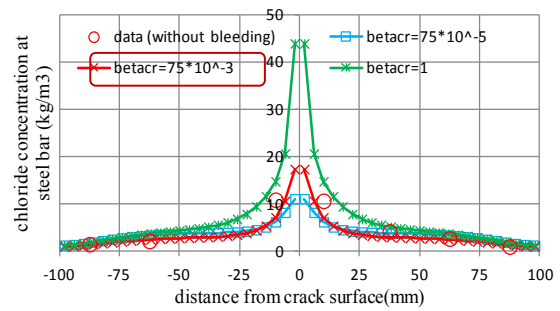


Fig. 8 - Chloride concentration along of reinforcing bar in concrete with various value of β_{cr} ($w = 0.15$ mm)

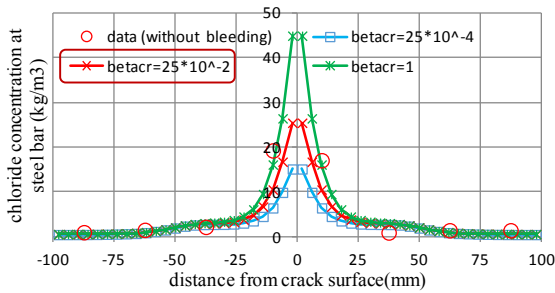


Fig. 9 - Chloride concentration along of reinforcing bar in concrete with various value of β_{cr} ($w = 0.5$ mm)

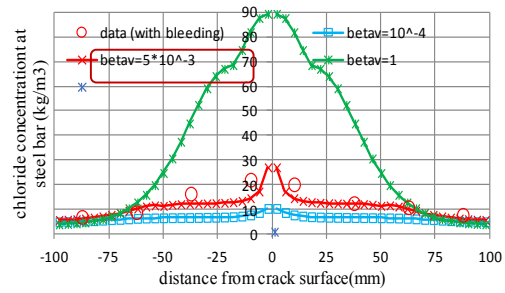


Fig. 10 - Chloride concentration along of reinforcing bar in concrete with various value of β_v ($w = 0.75$ mm, $v_w = 0.02$ mm)

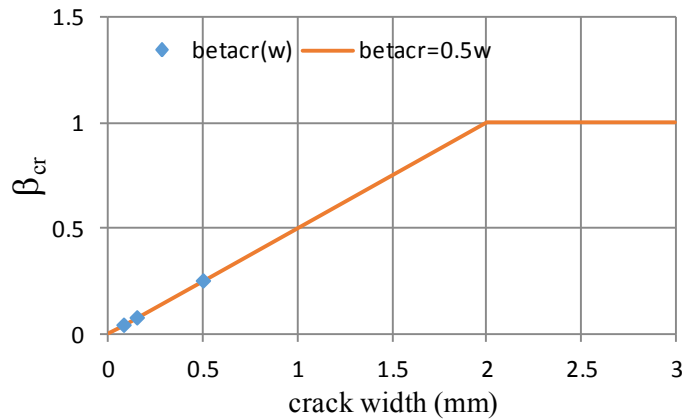


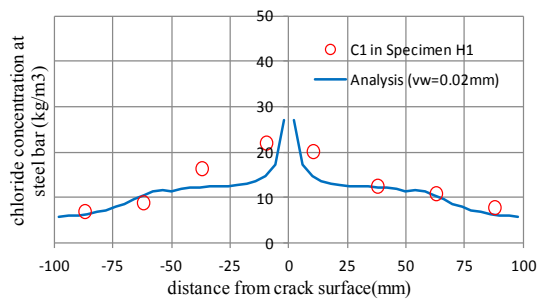
Fig. 11 - Relationship between β_{cr} and crack width

Table 4 - Material parameters

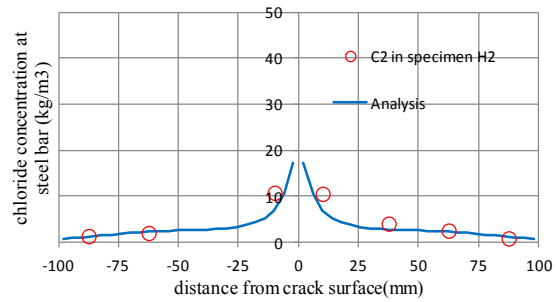
No.	V_0 (m ³ /m ³)	B	C	K_v	K_l	K_{lp}	K_{cl}
H1, H2, V1	0.15	14,000	0.5	0.05393	0.00108	0.03236	0.01079
V2	0.21	14,000	0.5	0.05393	0.00108	0.03236	0.01079

Table 5 - Conditions of specimens in numerical simulation

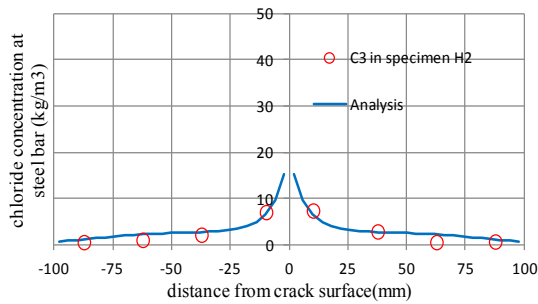
No	c (mm)	Crack width, w (mm)	Interfacial void, v_w (mm)	Crack interval, L (mm)	Dry-wet (days)	Time (days)
H1	40	0.75 (C1)	0.02	200	0.5-0.5	65
H2		0.15 (C2), 0.08 (C3)				
V1		0.08 (C4)	0			
V2		0.08 (C5)				



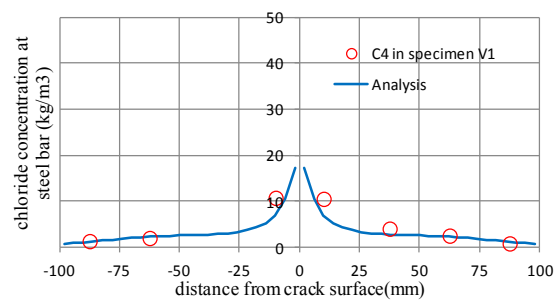
(a) C1 in Specimen H1 (w = 0.75 mm)



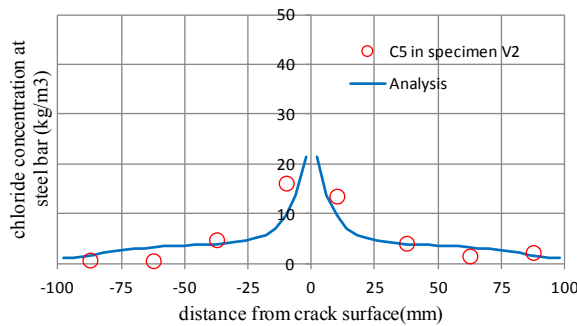
(b) C2 in Specimen H1 (w = 0.15 mm)



(c) C3 in Specimen H1 (w = 0.08 mm)



(d) C4 in Specimen V1 (w = 0.08 mm)



(e) C5 in Specimen V1 (w = 0.08 mm)

Fig. 12 - Comparison of experimental and analytical chloride concentration along reinforcing bar after 65 days of exposure

4. Evaluation of critical crack width based on numerical simulation

4.1 Method of evaluation

(1) Average chloride concentration at reinforcing bar

Chloride concentration along the reinforcement in concrete at each time $C(c, y)$ is obtained through numerical transport analysis. Average chloride content along reinforcement bar is considered as index of risk of reinforcement corrosion. Average chloride concentration at reinforcing steel bar C_{av} is calculated by averaging $C(c, y)$ with respect to position y for a crack interval:

$$C_{av} = \frac{1}{L} \int_0^L C(c, y) dy \quad (16)$$

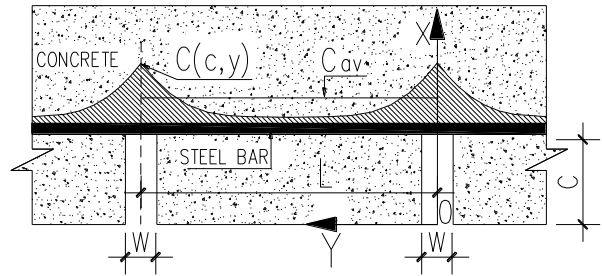
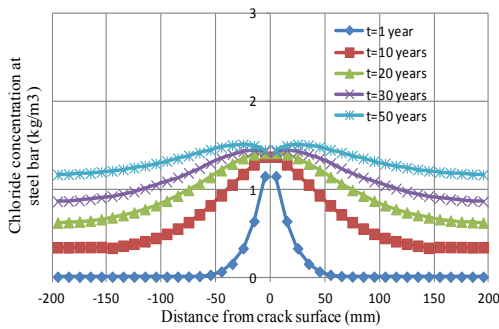
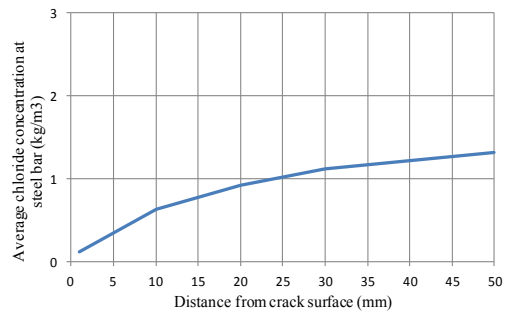


Fig. 13 - Determination of C_{av} by averaging method



(a) Calculated time-dependent chloride profile along the bar



(b) Calculated average chloride concentration at location of steel bar as a function of time

Fig. 14 - Determination of average chloride concentration at location of steel bar as a function of time

(2) Critical chloride concentration for onset of corrosion

Corrosion of reinforcement embedded in concrete is promoted by chloride, supplement of water and supplemental oxygen. In case of structures under chloride prone conditions such as coastal area affected by airborne salt, splash zone, and tidal zone, onset of corrosion is mainly governed by chloride concentration at the location of reinforcing bar. In the standard specification for concrete structures by Japan Society of Civil Engineers (JSCE), critical chloride concentration for initiation of steel corrosion C_{lim} (kg/m^3) is formulated as a function of type of cement and water-cement ratio of concrete. For ordinary Portland cement, it is expressed as:

$$C_{lim} = -3.0(W/C) + 3.4 \quad (17)$$

where W/C is water-cement ratio of concrete.

In this study, criteria of onset of corrosion is defined as

$$\frac{C_{av}}{C_{lim}} = 1 \quad (18)$$

where C_{av} is average chloride content at location of reinforcing bar.

(3) Critical crack width to prevent corrosion during service life

Based on numerical analysis, C_{av}/C_{lim} is evaluated as a function of time. It increases with increasing of time. Critical crack width is defined when C_{av}/C_{lim} becomes one at the end of service life of structure. If crack width is greater than the critical width, reinforcement corrosion will start within service life. Therefore, critical crack width depends on the expected service life of the structure. The smaller crack width should be restricted to, the longer service life is expected. In this study, 50 years of service life is assumed.

4.2 Cases of parametric sensitivity analysis of influencing factors on critical crack width

Table 6 shows influencing factors and their variation examined in the conducted sensitivity analysis. Environmental condition represented by drying-wetting cycle is examined because limitation of crack width in the JSCE standard specification (2002) is regulated depending on severeness of environmental condition. The influence of water-

cement ratio of concrete is considered in terms of pore size distribution, material parameters for transport of water and chloride ions in Chapter 2 and critical chloride concentration for initiation of steel corrosion. 43 cases shown in Table 7 are calculated in total.

Table 6 - Influencing factors examined and their variation

Influencing factors	Variations
Concrete cover, c (mm)	30, 50, 80
Water-cement ratio, W/C (%)	30, 45
Crack width, w (mm)	0, 0.05, 0.1, 0.2, 0.5, 1.0
Void width, v_w (mm)	0, 0.15
Environment condition (Drying-wetting cycle)	Tidal zone (2.85d D-0.15d W), splash zone (1.5d D-1.5d W)

Table 7 - Calculated cases in parametric sensitivity analysis

Case	W/C (%)	c (mm)	w (mm)	v_w (mm)	L (mm)	Dry-Wet (day)	Cav/Clim at 50 years
1	45	80	0	0	400	2.85-0.15	0.48
2	45	80	0.05	0	400		0.57
3	45	80	0.1	0	400		0.57
4	45	80	0.2	0	400		0.57
5	45	80	0.5	0	400		0.85
6	45	80	1	0	400		1.45
7	45	50	0	0	400		0.59
8	45	50	0.05	0	400		0.61
9	45	50	0.1	0	400		0.65
10	45	50	0.2	0	400		1.21
11	45	50	0.5	0	400		2.91
12	45	50	1	0	400		3.61
13	45	30	0	0	400		0.62
14	45	30	0.05	0	400		1.15
15	45	30	0.1	0	400		2.52
16	45	30	0.2	0	400		3.14
17	45	30	0.5	0	400		3.22
18	45	30	1	0	400		3.32
19	45	80	0	0.15	400		0.48
20	45	80	0.05	0.15	400		0.78
21	45	80	0.1	0.15	400		0.93
22	45	80	0.2	0.15	400		1.25
23	45	80	0.5	0.15	400	2.85-0.15	2.34
24	45	50	0	0.15	400		0.59
25	45	50	0.05	0.15	400		1.14
26	45	50	0.1	0.15	400		1.7
27	45	50	0.2	0.15	400		3.04
28	45	50	0.5	0.15	400		6.1
29	45	30	0	0.15	400		0.62
30	45	30	0.05	0.15	400		2.58
31	45	30	0.1	0.15	400		4.23
32	45	30	0.2	0.15	400		4.98
33	45	30	0.5	0.15	400	7.07	
34	45	50	0	0	400	1.5-1.5	0.7
35	45	50	0.05	0	400		0.93
36	45	50	0.1	0	400		1.51
37	45	50	0.2	0	400		1.7
38	45	50	0.5	0	400		1.71
39	30	50	0	0	400	2.85-0.15	0.32
40	30	50	0.05	0	400		0.44
41	30	50	0.1	0	400		0.5
42	30	50	0.2	0	400		0.83
43	30	50	0.5	0	400		1.23

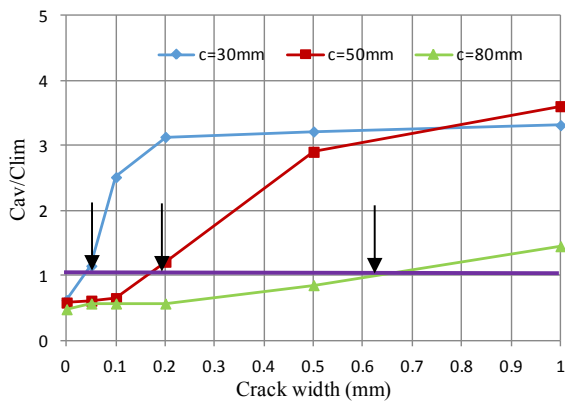


Fig. 15 – Chloride concentration at the location of reinforcing bar at 50 years (without interfacial void due to bleeding)

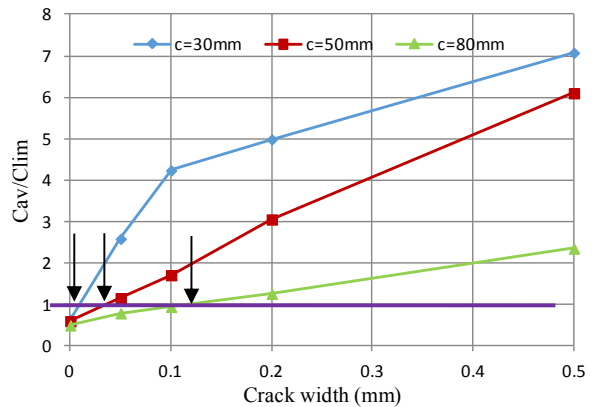


Fig. 16 - Chloride concentration at the location of reinforcing bar at 50 years (with interfacial void due to bleeding)

4.3 Analytical results of critical crack width

(1) Influence of cover thickness and interfacial void on critical crack width

Figures 15 and 16 show the relationship between crack width and calculated average chloride concentration at the location of reinforcing bar at 50 years with and without interfacial void around reinforcement due to bleeding respectively. Arrow indicates the point where average chloride concentration at the location of reinforcing bar reaches critical chloride concentration at 50 years. Crack width at this point is regarded as critical crack width to prevent corrosion during service life in terms of chloride ingress. In the series in Fig. 15, no interfacial void is provided around reinforcement. In series in Fig. 16, 0.15mm interfacial void due to bleeding is assumed. It is found in Fig. 15 that critical crack width is 0.05mm, 0.18mm, and 0.6mm in cases that cover thickness is 30mm, 50mm, and 80mm respectively. In Figure 16, critical crack width is 0.02mm, 0.05mm, and 0.13mm in cases that cover thickness is 30mm, 50mm, and 80mm respectively. The relationship between provided cover thickness and evaluated critical crack widths are plotted in Fig. 17. It can be seen in Fig. 17 that critical crack width increases with increasing of cover thickness in the series both with and without interfacial void. Critical crack width is decreased by the existence of interfacial void. This suggests that defect around steel bar due to bleeding should be avoided to make crack width control in RC member effective.

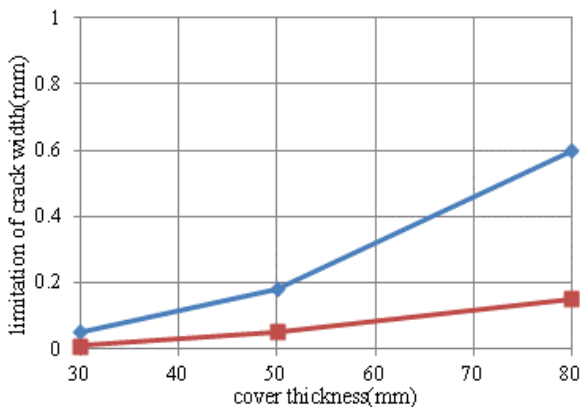


Fig. 17 - Evaluated critical crack width as a function of cover thickness

(2) Influence of environmental condition on critical crack width

Figure 18 shows the relationship between crack width and calculated average chloride concentration at the location of reinforcing bar at 50 years in tidal zone and splash zone. The tidal zones consist of 1.5 days of wetting and 1.5 days

of drying, while the splash zones consist of 2.85 days of wetting and 0.15 day of drying. It is found that critical crack width is 0.05mm in tidal zone and 0.18mm in splash zone respectively. It means that tidal zone is severer than splash zone for corrosion of reinforcement in concrete. This is because water and chloride penetration into concrete through crack increases with increasing of wetting period.

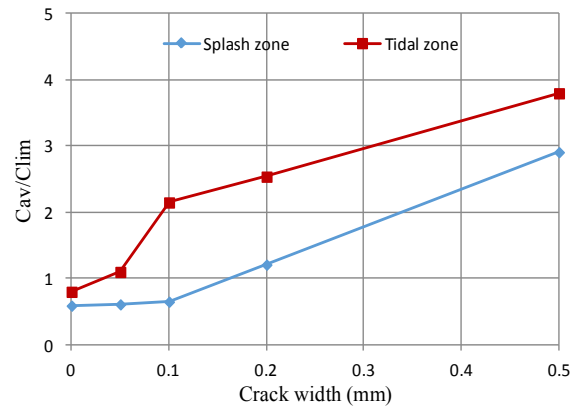


Fig. 18 - Chloride concentration at the location of reinforcing bar at 50 years in splash zone and tidal zone

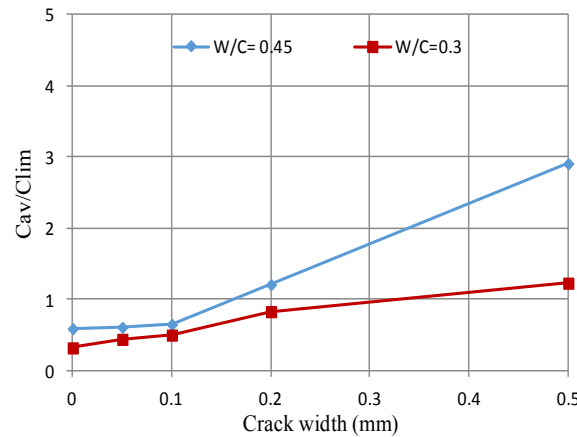


Fig. 19 - Chloride concentration at the location of reinforcing bar at 50 years for concrete of W/C = 0.3 and 0.45.

(3) Influence of water-cement ratio on critical crack width

Figure 19 shows the relationship between crack width and calculated average chloride concentration at the location of reinforcing bar at 50 years for concrete whose W/C is 0.3 and 0.45. It is found that critical crack width is 0.34mm and 0.18mm in cases that water-cement ratio is 30% and 45% respectively. It is suggested that, when concrete with higher water to cement ratio is used, crack width should be restricted more strictly to attain same level of durability.

5. Comparison of analytical critical crack width with those in design codes

Critical crack width or allowable crack width in several design codes is presented in Table 8.

Table 8 - Allowable crack width in design codes

Name of Standard	Crack width limitation (mm)
JSCE (2012)	$0.005c (< 0.5 \text{ mm})$
fib Model Code (2010)	$0.3 (c/40)$
BSI	0.3

In JSCE standard and fib Model Code, critical crack width is regulated as a function of cover thickness. Figure 20 shows the relationship between cover thickness and critical crack width by JSCE standard specification, fib Model Code, British Standards Institution and obtained by numerical simulation in this study. Compared with fib Model Code, analytically obtained critical crack width is close when cover thickness is 80mm, while the difference becomes greater when cover thickness is thinner. One of the reasons of this is that numerical simulation is carried out under drying-wetting condition, which is regarded severe condition for corrosion. Compared with JSCE standard, analytically obtained critical crack width is almost same when cover thickness is smaller than 60mm, the difference become greater when cover thickness is 80mm. In consequence, analytical critical crack width shows the tendency between JSCE standard and fib Model Code in both their value and dependency on cover thickness. Though critical crack width by BSI is constant value, it is almost same with average value of critical crack width by JSCE with respect to cover thickness. It was confirmed that the critical crack width that has been used in practical design is reasonable from the viewpoint of protection of reinforcement from ingress of aggressive agent.

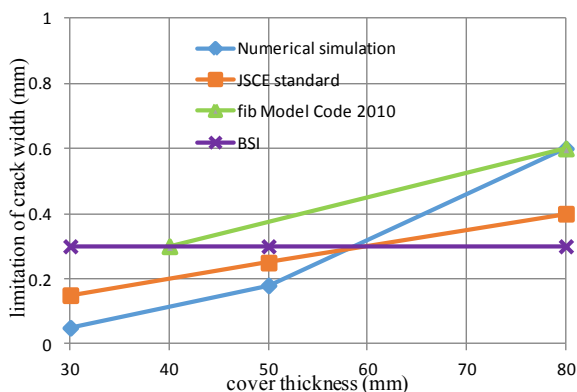


Fig. 20 - Relationship between critical crack width and cover thickness

6. Conclusions

Followings conclusions can be drawn from the conducted experiment and analysis:

- (1) It was experimentally confirmed that chloride ingress along reinforcement is accelerated by the existence of the interfacial void around reinforcement. The influence of interfacial void on chloride ingress along reinforcing bar became greater when crack width was great.
- (2) When concrete was cast parallel to steel bar, concrete near the casting surface became more porous than one far from casting surface due to bleeding effect.
- (3) Analytical method for chloride ingress into RC member, in which transport of water and chloride through flexural crack and the interfacial void around reinforcing bar are considered, was developed and verified by laboratory test. Chloride concentration at the location of steel bar increases with increasing of either crack width or width of interfacial void.
- (4) The results of the conducted parametric sensitivity analysis suggested that defect around reinforcement due to bleeding should be avoided in order to make the crack width control in RC member effective and crack width should be restricted more strictly to attain a same level of durability when concrete with higher water to cement ratio is used.
- (5) The critical crack width for corrosion of reinforcement in concrete evaluated by the numerical simulation showed similar tendency with critical crack widths in regulated in the design codes including JSCE standard specification. It was confirmed that the critical crack width that has been used in practical design is reasonable from the viewpoint of protection of reinforcement from ingress of aggressive agent.

Acknowledgement

The authors wish to express their gratitude to members of Concrete Laboratory in Nagaoka University of Technology. Especially thanks to Mr. Yamaguchi, Mr. Ohara, Mr. Ino and Mr. Minowa for kind helping and good working in experimental work.

References

1. E. Kato; Y. Kato; and T. Uomoto (2005) "Development of simulation model of chloride ion transportation in cracked concrete," Journal of

- Advanced Concrete Technology, 3(1), pp. 85-94.
2. Olga Garces Rodriguez and R. Doug Hooton (2003) "Influence of Cracks on Chloride Ingress into Concrete," *ACI Materials Journal*, 100(2), pp. 120-126.
 3. D.P. Bentz; E.J. Garboczi; Yang Lu; N.M. Aaron; R. Sakulich; and W. J. Weiss (2013) "Modeling of the Influence of Transverse Cracking on Chloride Penetration into Concrete," *Cement and Concrete Composites*, 38, pp. 65-74.
 4. Paulsson-Tralla J. and Silfwerbrand J. (2002) "Estimation of chloride ingress in uncracked and cracked concrete using measured surface concentrations," *ACI Materials Journal*, 99(1), pp. 27-36.
 5. Ishida T; Iqbal P.O.; and Anh H.T.L. (2009) "Modeling of chloride diffusivity coupled with non-linear binding capacity in sound and cracked concrete," *Cement and Concrete Research*, 39(10), pp. 913-23.
 6. R. François and G. Arliguie (1998) "Influence of service cracking on reinforcement corrosion," *J. Mater. Civil Eng.* 10(1), pp. 14-20.
 7. M. Sahmaran and I. Yaman (2008) "Influence of transverse crack width on reinforcement corrosion initiation and propagation in mortar beams," *Can. J. Civil Eng.* 35(3), pp. 236-245.
 8. N. Otsuki; S. Miyazato; N. Diola; and H. Suzuki (2000) "Influences of bending crack and water-cement ratio on chloride-induced corrosion of main reinforcing bars and stirrups," *ACI Mater. J.* 97(4), pp. 454-464.
 9. P. Schießl and M. Raupach (1997) "Laboratory studies and calculations on the influence of crack width on chloride-induced corrosion of steel in concrete," *ACI Mater J.* 94(1), 56-61.
 10. REHM, G. and H. MOLL (1965) "Experiments to Investigate the Influence of the Crack Width on the Formation of Rust on the Reinforcements of Reinforced," *Concrete Structural Parts, German Committee for Reinforced Concrete Report*, No. 170, pp.5-23.
 11. Shiessl, P. (1976) "Considerations on permissible crack width and optimum concrete layer in carbonated reinforced concrete structures," *Dtsch. Ausschuss Stahbeton*, No. 255, pp. 1-175.
 12. Shalon, R. et al (1964) "Corrosion of Reinforcing Steel in Hot Countries," *RILEM Bulletin*, No. 24, pp. 29-46.
 13. Okada, K. and Miyagawa, T. (1980) "Chloride corrosion of reinforcing steel in cracked concrete," *ACI Publication SP-65*, pp. 237-254.
 14. O'neil, E.F. (1980) "Study of reinforced concrete beams exposed to marine environment," *ACI Publication, SP-65*, pp. 113-132.
 15. Kamiyama, H. (1972) "Corrosion of reinforcement in concrete," *Cement and Concrete, JCA*, No. 308, pp. 50-57.
 16. Seki, H. and Maruyama, H. (1973) "Corrosion of steel bars at crack of reinforced concrete exposed to sea environments," *Report of The Port and Harbour Research Institute*, 12(3), pp. 203-225.
 17. M. Yachida; T. Ishibashi; and T. Satou (1987) "An investigation and study on cracking and corrosion of reinforced concrete bridge," *Proceeding of JSCE*, 378(6), pp. 195-202.
 18. Katawaki, K. (1977) "Corrosion of steel in concrete exposed to seawater spray zone," *Symposium proceeding on cracking of concrete structure*, pp. 133-136.
 19. Tarek Uddin Mohammed; Nobuaki Otsuki; Hidenori Hamada; and Toru Yamaji (2002) "Chloride-Induced Corrosion of Steel Bars in Concrete with Presence of Gap at Steel-Concrete Interface," *ACI Materials Journal*, 99(2), pp. 149-156.
 20. Savija, B.; Schlangen, E.; Pacheco, J.; Millar, S.; Eichler, T.; and Wilsch, G. (2014) "Chloride ingress in cracked concrete: a laser-induced breakdown spectroscopy (LIBS) study," *Journal of Advanced Concrete Technology*, 12(10), pp. 425-442.
 21. A. Castel; T. Vidal; R. François; and G. Arliguie (2003) "Influence of steel-concrete interface quality on reinforcement corrosion induced by chlorides," *Magazine of Concrete Research*, 55(2), pp. 151-159.
 22. Söylev, T.A. and François, R. (2003) "Quality of steel-concrete interface and corrosion of reinforcing steel," *Cement and Concrete Research*, 33(9), pp. 1407-1415.
 23. A. Michel; A.O.S. Solgaard; B.J. Pease; M.R. Geiker; H. Stang; and J.F. Olesen (2013) "Experimental investigation of the relation between damage at the concrete-steel interface and initiation of reinforcement corrosion in plain and fiber reinforced concrete," *Corrosion Science*, 77, pp. 308-321.
 24. Arliguie, G.; Castel, A.; Vidal, T.; and François, R. (2003) "Influence of steel-concrete interface quality on reinforcement corrosion induced by chlorides," *Magazine of Concrete Research*, 55(2), pp. 151-159.
 25. Tran, M.V.; Stitmannathum, B.; and Nawa, T. (2009) "Simulation of chloride penetration into concrete structures subjected to both cyclic

- flexural loads and tidal effects,” *Computer and Concrete*, 6(5), pp. 421-435.
26. Goto, Y. (1970) “Cracks formed in concrete around deformed tension bars,” *ACI Journal*, 68(4), pp. 35-47.
 27. N.T. Hien and T. Shimomura (2016) “Influence of initial defect of concrete due to bleeding on chloride ingress in RC member,” *The 7th International Conference of Asian Concrete Federation*, Ha Noi, Viet Nam, pp. 1-9.
 28. N.T. Hien; R. Ohara; and T. Shimomura (2017) “Influence of interfacial void around reinforcement due to bleeding on chloride ingress and its interaction with flexural crack,” *Proceedings of the Japan Concrete Institute*, 39(1), pp.781-786.
 29. JSCE (2012) “Standard Specification for Concrete Structures-2012 Design,” *Japan Society of Civil Engineers*.
 30. *Design of concrete structures CEB-FIP Model Code 1990*, Comite Euro-International du Beton.
 31. *Fib Model Code for Concrete Structures 2010*.
 32. *Building Code Requirements for Structural Concrete (ACI 318)*.
 33. *BS 8110-1 (1997) Structural use of concrete - Part 1: Code of practice for design and construction*, British Standards Institution.
 34. *Eurocode 2 (1992) Design of Concrete Structures. Part 1: General Rules and Rules for Buildings*, European Committee for Standardisation.
 35. T. Shimomura and K. Maekawa (1977) “Analysis of the drying shrinkage behavior of concrete using a micromechanical model based on the microspore structure of concrete,” *Magazine of Concrete Research*, 49(181), pp. 303-322.
 36. S. Kobayashi and T. Shimomura, (2002) “Numerical Analysis on Transport of Aggressive Materials and Corrosion of Steel Bars in Concrete,” *Proceedings of the Japan Concrete Institute*, 24(1), pp. 831-836.
 37. Maruya, T.; Somnuk, T.; and Matsuoka, Y. (1994) “Simulation of chloride penetration into hardened concrete,” *Proceedings of the CANMET/ACI International Conference of Durability of Concrete*, pp. 519-538.
 38. H.T. Thynn and T. Shimomura. (2009) “Hybrid computational method for capillary suction and nonsaturated diffusion in concrete,” *4th International Conference on Construction Materials ConMat'09*, pp. 1075-1080.